Pergamon

Int. J. Heat Mass Transfer. Vol. 37, No. 5, pp. 771–782, 1994

0017–9310/94 $6.00 + 0.00

A dynamic thermal insulator: inducing resonance within a fluid saturated porous medium enclosure heated periodically from the side

B. V. ANTOHE and J. L. LAGE

Mechanical Engineering Department, Southern Methodist University, Dallas, TX 75275-0335, U.S.A.

(*Received* 28 *April* 1993 *and in final form* 24 *September* 1993)

Abstract—This theoretical and numerical study investigates the natural convection flow within a fluid saturated porous medium enclosure subjected to intermittent heating from the side (hot wall). A theory for predicting the natural convection frequency of the flow wheel circulating inside the enclosure is developed from the general porous medium equations on a scaling basis. Physical insight indicates that heat flow resonance might occur when the input heat frequency matches the flow wheel circulating frequency. Numerical simulations confirm the existence of a preferred (resonance) input heat pulsating frequency. They also reveal that at the resonance frequency the fluid saturated porous medium system behaves as a *dynamic thermal insulator* in which the strong natural convection activity within the system, characterized by high amplitude heat flow oscillations, coexists with a damped oscillatory heat flux at the isothermal (cold) wall.

1. INTRODUCTION

ALTHOUGH most of the known phenomena in natural convection systems are induced by transient effects, only a small number of studies published in the archival literature considered transient boundary conditions.

Systems with transient thermal boundary conditions differ from classical transient natural convection problems in which the *transient* relates to the fluid flow response to a single (instantaneous) change in thermal boundary conditions. An excellent review, with numerical and experimental results considering a clear fluid system (one with no porous matrix), was offered by Patterson and Armfield [1]. Considering a fluid saturated porous medium enclosure, the transient heat transfer development caused by a step change in vertical wall temperatures was studied by Poulikakos and Bejan [2], assuming Darcy flow model (steady). The analysis was extended later on by Poulikakos and Bejan [3], for higher Rayleigh numbers, with the addition of a quadratic drag term in the momentum equation. Another similar transient case, involving simultaneous heat and mass transfer, was studied by Gross *et al.* [4] assuming a step change in temperature and concentration boundary conditions of a vertical surface.

It is worth noting that the steady flow model used in the porous medium studies cited in the previous paragraph is supported by Nield and Bejan [5] who indicated that in most practical situations the transient flow inertia decay is very short and can be neglected. This is also verified by the theoretical analysis of transient natural convection within an enclosure with constant boundary conditions presented by Lage [6], where the time decay scale is shown to be proportional to the Darcy number divided by the porous modified Prandtl number.

Natural convection problems with time dependent thermal boundary conditions have been studied only very recently and the analyses have been limited so far to clear fluid systems. A rectangular enclosure subjected to oscillatory (sinusoidal) temperature at one vertical wall was studied by Yang *et al.* [7] and by Kazmierczak and Chinoda [8]. Lage and Bejan [9] investigated the critical frequency for natural convection resonance in a fluid enclosure subjected to intermittent heat flux from the side. Mantle *et al.* [10] reported experimental results for a shallow rectangular enclosure (aspect ratio 1 : 4) heated periodically from the bottom and cooled at constant temperature from the top. Their results showed an increase of up to 12% in the heat transfer through the enclosure as compared with the steady state heat transfer.

The present study investigates, theoretically and numerically, the time evolution of flow and temperature fields within a fluid saturated porous medium enclosure. The enclosure is heated periodically from one side wall with the opposite side wall maintained at a constant temperature and all other surfaces insulated. The focus here is on detecting natural convection resonance within the enclosure. The search for the resonant state is carried out by increasing the heat pulsating frequency and observing the time evolution of the surface averaged heat flux crossing the mid section of the enclosure (note that this heat flux is strongly related to the natural convection activity within the enclosure). The resonance frequency is defined as the frequency that leads to a local maximum

NOMENCLATURE

Da	Darcy number, equation (7)
f, F	dimensional and nondimensional frequencies, $F = 1/(2\Omega)$
g	gravitational acceleration
H	enclosure height
i	iteration count index
I	Forchheimer inertia coefficient, equation (8)
L	enclosure length
J	viscosity ratio, equation (6)
k	thermal conductivity
K	permeability
Nu	Nusselt number, equations (10), (11)
p, P	dimensional and nondimensional pressures, equation (5)
Pr	Prandtl number, equation (7)
q'', Q''	dimensional and nondimensional heat fluxes, equation (8)
Ra	Rayleigh number, equation (8)
t	time
T	temperature
u, v	horizontal and vertical seepage (Darcy) velocity components
U, V	nondimensional horizontal and vertical velocity components, equation (5)
x, y	horizontal and vertical coordinates
X, Y	nondimensional horizontal and vertical coordinates, equation (5)
W	nondimensional volume averaged velocity, equation (21).

Greek symbols

α	thermal diffusivity, equation (7)
β	isobaric coefficient of thermal compressibility
δ	velocity layer thickness scale
ε	dummy variable, equation (13)
θ	nondimensional temperature, equation (6)
λ	volumetric specific heat, equation (7)
μ	dynamic viscosity
ν	kinematic viscosity
ρ	density
τ	nondimensional time, equation (6)
υ	local (i, j) volume
ϕ	porosity
Ψ	streamfunction
Ω	nondimensional half period of heat pulsation.

Subscripts

c	isothermal (cold)
cr	critical
D	porous modified
ΔT	temperature difference based
f	fluid
h	hot
m	mid vertical plane
M	reference value
max	maximum value
s	porous medium (fluid and solid matrix)
ss	steady state
v	flow
o	initial.

Superscript

$\bar{(\ )}$	surface averaged.

surface averaged heat flux amplitude from the zero frequency amplitude limit.

The numerical simulations cover a wide range of input heat frequency with Darcy number varying from 10^{-2} to 10^{-6}. The maximum Rayleigh number reported in each case is constrained by the CPU time necessary to obtain meaningful (accurate) results.

Besides the fundamental theoretical aspect of this work, numerous engineering applications involving fluid saturated porous medium warrant its pursuit, for instance in the areas of: building insulation and fire protection techniques [11, 12], phase change processes [13, 14], hazardous thermo-chemical spreading [15], and advanced energy systems for space application [16, 17].

2. FORMULATION OF THE PROBLEM

The physical model of the problem discussed in this study is synthesized in Fig. 1, where a rectangular porous matrix enclosure saturated with fluid is depicted (top). The nondimensional time dependent general conservation of mass, momentum and energy equations for a porous medium [18, 19], written in Cartesian coordinates, are

$$\frac{\partial U}{\partial X}+\frac{\partial V}{\partial Y}=0 \tag{1}$$

$$\frac{\mathrm{D}U}{\mathrm{D}\tau}=-\frac{\partial P}{\partial X}+\phi\, Pr\, J\nabla^2 U - \phi^2\frac{I}{Da}(U^2+V^2)^{1/2}U-\phi^2\frac{Pr}{Da}U \tag{2}$$

$$\frac{\mathrm{D}V}{\mathrm{D}\tau}=-\frac{\partial P}{\partial Y}+\phi\, Pr\, J\nabla^2 V+\phi^2\frac{I}{Da}(U^2+V^2)^{1/2}V - \phi^2\frac{Pr}{Da}V+\phi^2\, Ra\, Pr\,\theta \tag{3}$$

$$\frac{\lambda}{\phi}\frac{\partial\theta}{\partial\tau}+U\frac{\partial\theta}{\partial X}+V\frac{\partial\theta}{\partial Y}=\nabla^2\theta. \tag{4}$$

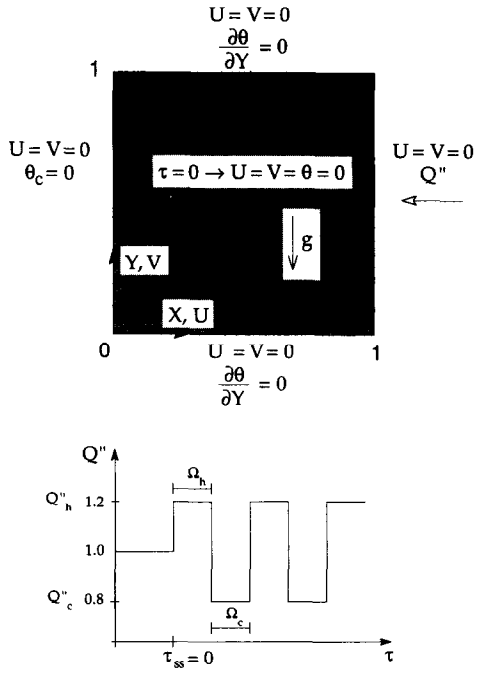

FIG. 1. Rectangular fluid saturated porous medium enclosure with boundary and initial conditions.

In writing equations (1)–(4) it is implicitly assumed that the porous matrix is saturated with a Newtonian fluid with constant properties. The Oberbeck–Boussinesq approximation is applied, with fluid and porous matrix being in thermal equilibrium. The term $D()/D\tau$ of equations (2) and (3) represents the total derivative, $\partial()/\partial\tau + U\,\partial()/\partial X + V\,\partial()/\partial Y$. Nondimensional variables, with corresponding dimensional quantities listed in the Nomenclature, are

$$(X, Y) = \frac{(x, y)}{H} \quad (U, V) = \frac{(u, v)}{\alpha_s/H}$$

$$P = (p + \rho g y)\frac{\phi^2 H^2}{\rho \alpha_s^2} \tag{5}$$

$$\theta = \frac{T - T_0}{q''_M H/k_s} \quad \tau = \frac{t - t_{ss}}{\phi H^2/\alpha_s} \quad J = \frac{\mu_s}{\mu} \tag{6}$$

$$\lambda = \frac{(\rho c)_s}{(\rho c)_f} \quad Pr = \frac{\nu}{\alpha_s} \quad \alpha_s = \frac{k_s}{(\rho c)_f} \quad Da = \frac{K}{H^2} \tag{7}$$

$$Ra = \frac{g\beta q''_M H^4}{\nu \alpha_s k_s} \quad I = 1.75\left(\frac{Da}{150\phi^3}\right)^{1/2} \quad Q'' = \frac{q''}{q''_M}. \tag{8}$$

Parameter J, equation (6), accounts for the effective viscosity of the fluid saturated porous medium [20]. The expression for the inertia parameter, I, shown in equation (8), is obtained by invoking the Ergun [21] model. The porous modified heat flux based Rayleigh number, Ra_D, is defined as equal to the product $RaDa$.

Observe that the Rayleigh number defined in equation (8) is based on a reference value of the pulsating heat flux, q''_M. The instantaneous time dependent Rayleigh number is then equal to RaQ''.

The inertia time dependent term kept in both momentum equations (2) and (3), as mentioned previously, is negligible in most practical situations provided the Darcy number is small. Through scale analysis [6], it is possible to show that the transient decay time is proportional to $Da/(\phi^2 Pr)$ for Darcy flow, and $Da^{3/4}/(\phi^{3/2} Ra_D Pr)^{1/2}$ for Forchheimer flow. It follows that for high Darcy number values, as considered in the present study, the transient flow inertia terms should not be neglected, a priori.

The porous medium enclosure is saturated initially with motionless and isothermal fluid. During the entire thermal process, the left wall of the enclosure is maintained at a constant temperature, θ_c, equal to the initial fluid saturated porous medium temperature, $\theta_0 = 0$ (Fig. 1). A constant heat flux, $Q'' = 1$, is then imposed at the right wall. The first phase of the thermal process refers to the heating of the enclosed quiescent fluid until a steady convection regime is attained. At $\tau = 0$ (note that the nondimensional time, equation (6), is zero when the system reaches steady state, $t = t_{ss}$), the system undergoes a second phase during which the input heat flux pulsates in time around its reference value.

Here, the heat pulsation half-amplitude is kept at 20% of the reference value. Equal heating and cooling periods are assumed, $\Omega_h = \Omega_c = \Omega$, so the nondimensional heat pulsating frequency is: $F = 1/(2\Omega)$. According to the definition of dimensionless time, equation (6), the dimensional heating and cooling periods are, respectively: $(t_h, t_c) = (\Omega_h, \Omega_c)\phi H^2/\alpha_s$.

Three parameters are chosen to help understand the thermal convective effect of pulsating heat, respectively: right (heating) wall instantaneous surface averaged temperature, $\bar{T}_h$; instantaneous surface averaged left (isothermal) wall heat flux, $\bar{q}''_c$; and instantaneous surface averaged heat transfer rate through an imaginary vertical plane positioned at the middle of the enclosure, $\bar{q}''_m$. The corresponding nondimensional quantities are

$$\bar{\theta}_h = \int_0^1 \theta|_{X=1}\,dY \tag{9}$$

$$Nu_c = \frac{\bar{q}''_c}{q''_M} = \int_0^1 \left.\frac{\partial\theta}{\partial X}\right|_{X=0} dY \tag{10}$$

$$Nu_m = \frac{\bar{q}''_m/H}{q''_M} = \int_0^1 \left[(RaPr)^{1/2} U\theta - \left.\frac{\partial\theta}{\partial X}\right]_{X=1/2} dY. \tag{11}$$

It is worth noting that a temperature based Rayleigh number can be defined and written as

$$Ra_{\Delta T} = \frac{g\beta(\bar{T}_h - T_c)H^3}{\nu\alpha_s} = \bar{\theta}_h Ra. \tag{12}$$

3. NUMERICAL METHOD

Numerical simulations are performed by solving the system of time dependent differential equations

(1)–(4), with appropriate boundary and initial conditions, using the finite volume method [22]. This method was previously applied and validated for similar problems (e.g. refs. [8, 9, 23]). The discretized equations are solved using the SIMPLE algorithm [22] with implicit alternating-direction Gauss–Seidel iterative method, and the efficient Tri-Diagonal-Matrix Thomas algorithm. The present numerical code is validated also against results reported by Armfield and Patterson [24].

Extensive grid accuracy tests are performed, following the same basic concepts described in detail by Manole and Lage [25]. Several different grid distributions are implemented, depending on the case, using 60 by 60 grid lines. Numerical results reported here are at least 5% accurate considering a 50% increase in the total number of grid lines.

Numerical convergence is examined locally following the criterion

$$\mathrm{MAX}\left|\frac{\varepsilon^{i+1}-\varepsilon^{i}}{\varepsilon^{i}}\right| < 10^{-3} \tag{13}$$

where ε is replaced by U, V, and θ at every (X, Y) location of the discretized domain, and i and $i+1$ are two consecutive iterations at the same time τ.

Time step selection follows the same procedure detailed by Lage and Bejan [9]. Here, the minimum number of iterations per cycle was conservatively set at 400 with results being insensitive to any further decrease in time step.

4. THEORETICAL ANALYSIS

The parameter space of the present problem is considerably large. Even considering a specific case, fixing all parameters but the heat pulsating frequency, the probability of choosing an input heat frequency near the resonance frequency is very small. In this section, a theory based on scale analysis is developed to obtain an estimate for the input heat pulsating frequency that leads to natural convection resonance. The result of this simple but powerful analysis is fundamental to limit the frequency range for determining numerically the precise resonance frequency value.

As mentioned before, resonance is expected to be induced when the heat pulsating frequency, f, coincides with the frequency of the flow wheel circulating within the enclosure, f_v,

$$f_v = f. \tag{14}$$

Equation (14) is a mathematical representation of a continuous thermal charging process. Consider a fluid pack circulating within the enclosure with a certain frequency such that when it gets close to the heating wall, at every cycle, the heat flux is at the same strength (e.g. heating). For that to happen, it is necessary that the circulating fluid pack and pulsating heat have the same frequency.

If the energy absorbed by the fluid pack from the heating wall is completely delivered to the isothermal wall, the system will operate as a continuous heat transmitter with isothermal wall heat flux wave following the heating wall heat flux wave with similar amplitude and a phase shift (due to the system's thermal inertia). Otherwise, the energy will accumulate inside the circulating fluid pack, increasing its temperature and creating conditions for heat convection resonance due to the pulsating nature of the heat input. The energy accumulated by the fluid pack might eventually be returned to the heating wall during its cooling period. In this case the system will operate as a *dynamic thermal insulator* in which the heat oscillation at the heating wall is not felt by the isothermal wall (obviously during the periodic steady regime the cycle averaged heat flux at the heating wall matches the cycle averaged heat flux at the isothermal wall).

Furthermore, it is reasonable to expect that higher fluid velocities inside the enclosure (high Ra) improve the conditions for resonance: the fluid pack carrying high energy would have less time to deliver this energy to the isothermal wall as compared with another circulating fluid pack flowing synchronously with the cooling period of the input heat pulse (this fluid pack will tend to flow slower).

The task now is to obtain a proper representation for the flow wheel frequency, f_v. In dimensional form, the circulating frequency scale is obtained by dividing the fluid velocity scale by the enclosure perimeter (scaled distance traveled by a fluid pack per cycle within the enclosure)

$$f_v \sim \frac{v}{2(H+L)}. \tag{15}$$

For a square cavity, as considered in here, $L = H$, so the flow frequency written in nondimensional form becomes

$$F_v \sim \frac{\phi V}{4}. \tag{16}$$

The velocity scale, V, is obtained by first cross differentiating the steady version of the general momentum equations (2) and (3) to eliminate pressure. The result, in a scale form, is

$$V^2 \sim -\phi J Pr \frac{V}{\delta^2} + \frac{0.143\phi^{1/2}}{Da^{1/2}} V^2 + \frac{\phi^2 Pr}{Da} V + \phi^2 Ra\, Pr\, \theta. \tag{17}$$

The quadratic equation in V, equation (17), can be solved directly. After some manipulation (see Lage [26] for details) the scale for V is obtained as

$$V \sim \frac{-\Pi + \left[\Pi^2 + 4\theta\phi^2 Ra\, Pr \times \left(1 + \phi J Pr A(Pr) + \frac{0.143\phi^{1/2}}{Da^{1/2}}\right)\right]^{1/2}}{2\left(1 + \phi J Pr A(Pr) + \frac{0.143\phi^{1/2}}{Da^{1/2}}\right)} \tag{18}$$

where $A(Pr)$ is equal to 1 for $Pr \geqslant 1$, or to Pr^{-1} for $Pr \leqslant 1$, and $\Pi = \phi^2 Pr/Da$. Notice that here the temperature inside the enclosure, θ, scales with the unknown $\bar{\theta}_h$ value (recall θ_c is zero). However, it is possible to obtain an approximate scale for θ, considering the simple Darcy regime or the Forchheimer-extended Darcy regime [5, 9]. The latter is chosen here since thermal resonance is a phenomenon related with high Rayleigh number flow, so

$$\bar{\theta}_h \sim \frac{1}{(Ra\,Da)^{1/5}}. \tag{19}$$

Replacing θ in equation (18) with $\bar{\theta}_h$, equation (19), and substituting the result in equation (16) results in

$$F_v \sim \frac{-\Pi\phi + \phi\left[\Pi^2 + 4\phi^2 Ra^{4/5} Da^{-1/5} Pr \times \left(1 + \phi J Pr A(Pr) + \frac{0.143\phi^{1/2}}{Da^{1/2}}\right)\right]^{1/2}}{8\left(1 + \phi J Pr A(Pr) + \frac{0.143\phi^{1/2}}{Da^{1/2}}\right)}. \tag{20}$$

It is worth noting that equation (20) provides us with one unique expression for F_v, valid within the entire range covered by the general momentum equations. This result extends the theoretical analysis performed by Lage and Bejan [9] who considered two simpler cases, namely Darcy and Forchheimer-extended Darcy flows, separately. Equation (20) also matches the result for clear fluid system [9] by simply dropping the terms related to the porous medium model.

5. RESULTS AND DISCUSSIONS

Numerical results are obtained considering a fluid saturated porous medium with $\phi = 0.4$, $\lambda = 0.4$, $Pr = 7$, and $J = 1$. The time evolution of thermal parameters is presented in Figs. 2 and 3. In each figure, the middle graph refers to the input heat resonance frequency.

Figures 2(a) and (b) are for $Da = 10^{-2}$. In Fig. 2(a), for $Ra = 10^6$, three cases with increasing heat pulsating frequency from top to bottom are depicted. Evidently, the heat transfer mechanism inside the enclosure varies as the heat frequency increases. The top graph, for $F = 10$, shows the isothermal wall non-dimensional heat flux, Nu_c, trailing the non-dimensional mid-plane heat flow, Nu_m, with a phase shift. The phase shift, caused by the flow wheel inertia, is even more evident on the middle graph for $F = 33.3$. Furthermore, as the frequency increases from 10 to

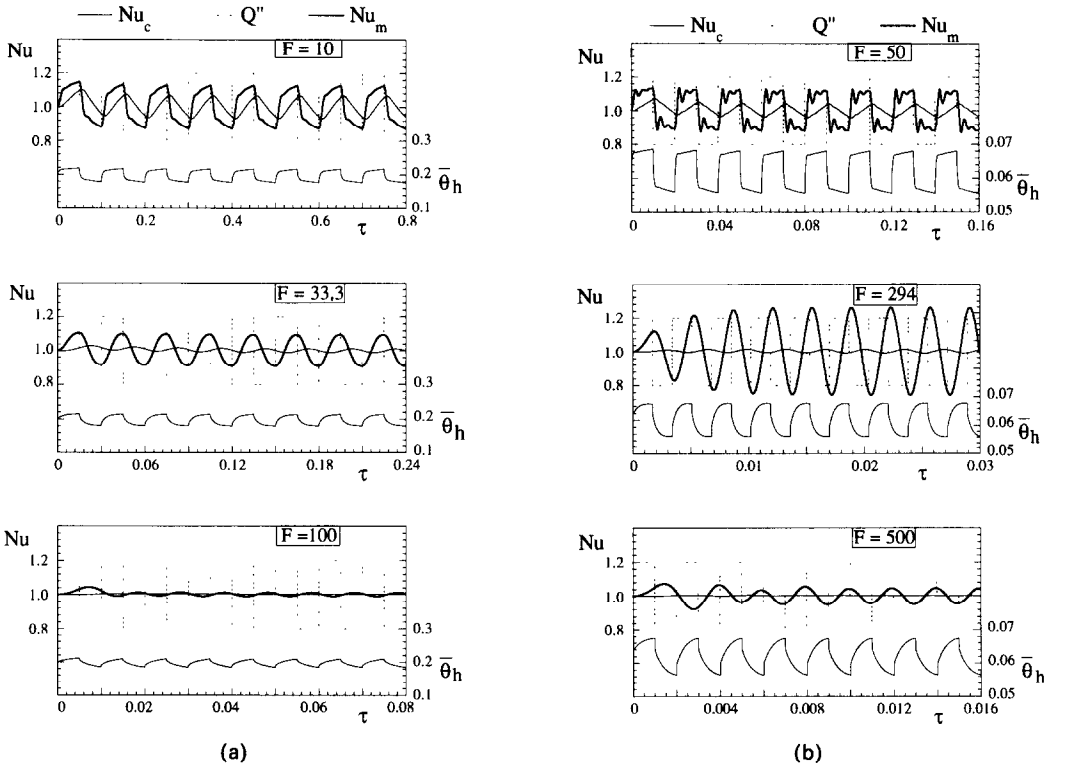

FIG. 2. Time evolution of thermal parameters for three input heat frequencies (middle graph is for *resonance* frequency), and $Da = 10^{-2}$. (a) $Ra = 10^6$; (b) $Ra = 10^8$.

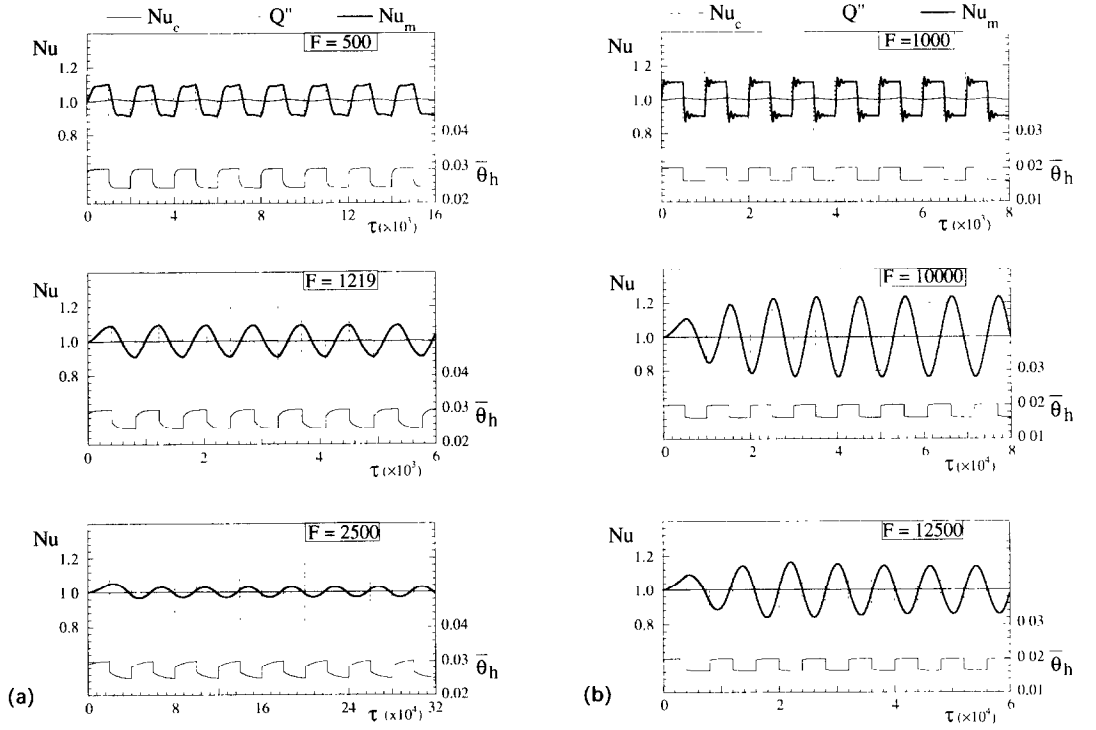

FIG. 3. Time evolution of thermal parameters for three input heat frequencies (middle graph is for *resonance* frequency), and $Da = 10^{-4}$. (a) $Ra = 10^{10}$; (b) $Ra = 10^{12}$.

33.3, the isothermal wall heat flux amplitude is reduced more abruptly than the mid-plane heat flux indicating a decrease in the energy being delivered by the hot fluid stream (flowing synchronously with the heating phase of the heating wall) to the isothermal wall, a situation favorable to resonance. A further increase in frequency (lower graph $F = 100$) indicates a reduction in both isothermal wall and mid-plane heat flux amplitudes. This heating frequency is too high for the system to react.

In Fig. 2(b), for $Ra = 10^8$, the system responds to an increase in heat pulsating frequency in a similar fashion. However, the middle graph, for $F = 294$, clearly indicates stronger flow resonance within the enclosure (notice Nu_m amplitude higher than Q'' amplitude). Although in this case the amplitude of the isothermal wall heat flux is also reduced (Nu_c flattens) as F increases, the Nu_m amplitude value clearly increases and decreases as F goes from 50 to 294 and from 294 to 500, respectively. An interesting detail, not so evident in Fig. 2(a), is the abnormal behavior of Nu_m for low frequency, $F = 50$. The heat flow crossing the mid plane of the enclosure oscillates within each heating period. This oscillation is related to the natural frequency of the convective flow within the porous medium enclosure.

Figures 3(a) and (b) for $Da = 10^{-4}$, and, respectively, $Ra = 10^{10}$ and 10^{12}, indicate the same essentials as Figs. 2(a) and (b). Notice, however, the higher frequencies and the almost square shape of the surface averaged heating wall temperature. The resonance at $F = 10^4$ (Fig. 3(b)) is not as pronounced as the one obtained for $Da = 10^{-2}$, $Ra = 10^8$ and $F = 294$ (Fig. 2(b)). This results from the damping imposed by the less permeable porous matrix (lower Da).

A summary of the numerical exercise performed to detect resonance is presented in Fig. 4, for $Da = 10^{-2}$ (top) and 10^{-4} (bottom) and several Rayleigh

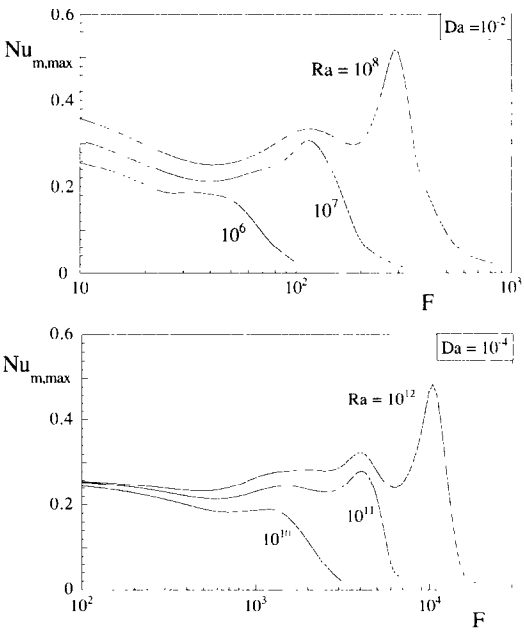

FIG. 4. Maximum amplitude of mid plane heat flow vs input heat pulsating frequency. Top: $Da = 10^{-2}$; bottom: $Da = 10^{-4}$.

numbers. Plotted in the ordinate is the maximum amplitude of the oscillatory mid plane Nusselt number, $Nu_{m,max}$, during one heating cycle after periodic steady regime is achieved. Notice that for the low frequency range ($F < 20$, top graph) $Nu_{m,max}$ values move upward tending to the steady state value equal to 0.4 (exact for $F \to 0$). As frequency increases, $Nu_{m,max}$ decreases up to a certain value beyond which the resonance effect sets in forcing its value to increase. Evidently, as F increases further on ($F \to \infty$) the system response dies out as indicated by $Nu_{m,max}$ value tending to zero in all cases.

Common to both graphs in Fig. 4 is the appearance of additional $Nu_{m,max}$ peaks, with the curve for one specific Rayleigh number following the shape of the lower Rayleigh number curves. This indicates the existence of more than one *resonance mode* for high Rayleigh numbers. Note that as Darcy number is reduced the system becomes less susceptible to resonance, as indicated by the higher Ra_{Da} (bottom graph) needed to achieve approximately the same $Nu_{m,max}$ resonance amplitude of the top graph. Reducing the Darcy number further to 10^{-6} results in no resonance at all, with $Nu_{m,max}$ curves indicating a monotonic decrease as frequency increases, for Ra as large as 10^{13}.

Results shown in Fig. 4 are for situations when a periodic steady regime is attained. The number of necessary cycles needed for achieving this regime depends on the case. Figure 5 presents phase-plane portrayed for each of the three cases depicted in Fig. 2(b). These figures show the evolution of the convection flow towards a periodic steady regime within the enclosure. The nondimensional volume averaged velocity within the computational domain, defined as

$$W = \sum_{i,j} \vartheta_{ij}(U(i,j)^2 + V(i,j)^2)^{1/2} \qquad (21)$$

is plotted vs the surface averaged heating wall temperature. In Fig. 5, the arrows indicate the starting point of the heat pulsating process. Notice that the middle graph presents the largest area within the W vs $\bar{\theta}_h$ curve (largest W range), a fact consistent with the resonance phenomenon. Also, the wiggles shown in the top graph ($\bar{\theta}_h$ extremes) indicate the oscillatory process within each cycle, the same phenomenon already discussed in connection with Fig. 2(b).

Table 1 presents a comparison between numerical and theoretical (predicted) resonance frequencies from equation (20). As expected, the theoretical values are off by a factor of order 1, being consistently smaller. Theoretical resonance frequency values for

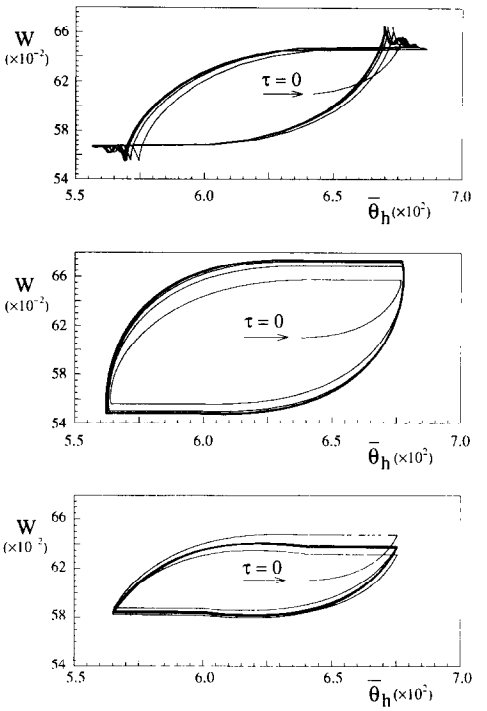

FIG. 5. Average velocity vs average heating wall temperature for $Da = 10^{-2}$ and $Ra = 10^8$. Top: $F = 50$; middle: $F = 296$ (resonance); bottom: $F = 500$.

$Da = 10^{-6}$ are included for reference only since, as indicated in the table, no resonance was observed in the numerical simulations.

Finally, Figs. 6(a) and (b) and 7(a) and (b), present streamlines and isotherms, respectively, for $Ra = 10^8$, $Da = 10^{-2}$, $F = 294$, and $Ra = 10^{12}$, $Da = 10^{-4}$, $F = 10^4$. In both cases, the natural convection flow evolves from picture 1 (start heating) to 6 (start cooling) in a steady periodic fashion. For each case, the complete sequence of streamline pictures is prepared using the same streamfunction maximum and minimum values (streamfunction defined, as usual, as $U = \partial\Psi/\partial Y$ and $V = -\partial\Psi/\partial X$). So in Fig. 6(a) for instance, it is possible to observe the strengthening of the flow during the heating phase by following the sequence 1–6 (notice the increase in the number of streamlines from 6, in picture 1, to 8, in picture 6) and the weakening of the flow during the cooling phase, sequence 6–1. The same can be observed in Fig. 7(a). From both Figs. 6(a) and 7(a), it is possible to conclude that the scale used for the distance travelled by a fluid pack circulating within the enclosure represents

Table 1. Comparison between numerical and theoretical resonance frequencies ($\phi = 0.4$, $\lambda = 0.4$, $J = 1$, $Pr = 7$)

Da	10^{-2}			10^{-4}			10^{-6}	
Ra	10^6	10^7	10^8	10^{10}	10^{11}	10^{12}	10^{12}	10^{13}
Numerical	33	114	294	1219	4000	10000	—	—
Theoretical	18.3	47.6	121.4	699.4	1820.1	4636.7	2207.8	6309.8

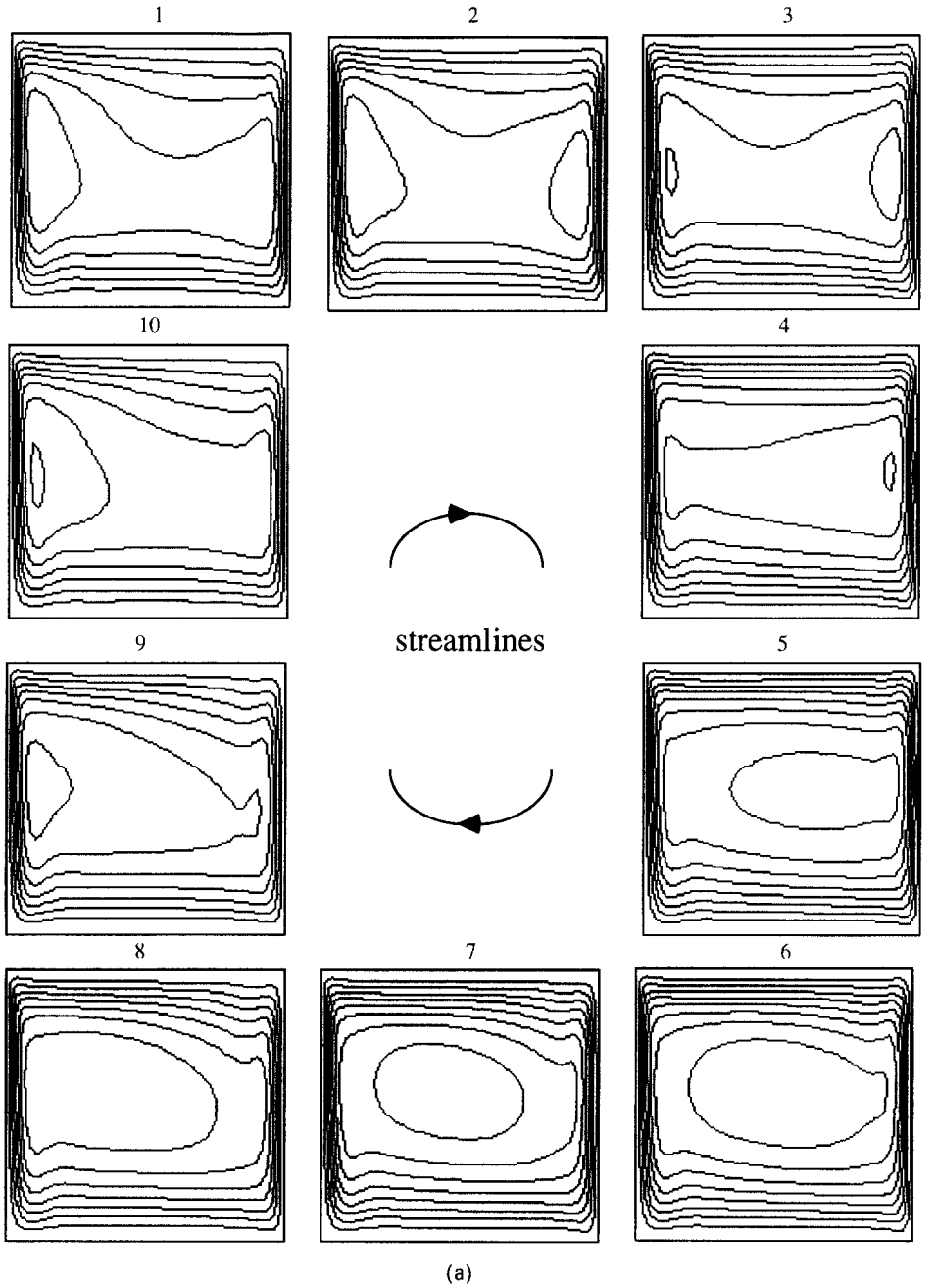

FIG. 6. Isolines from numerical simulations for $Da = 10^{-2}$, $Ra = 10^{8}$, and $F = 294$. (a) Streamlines; (b) isotherms.

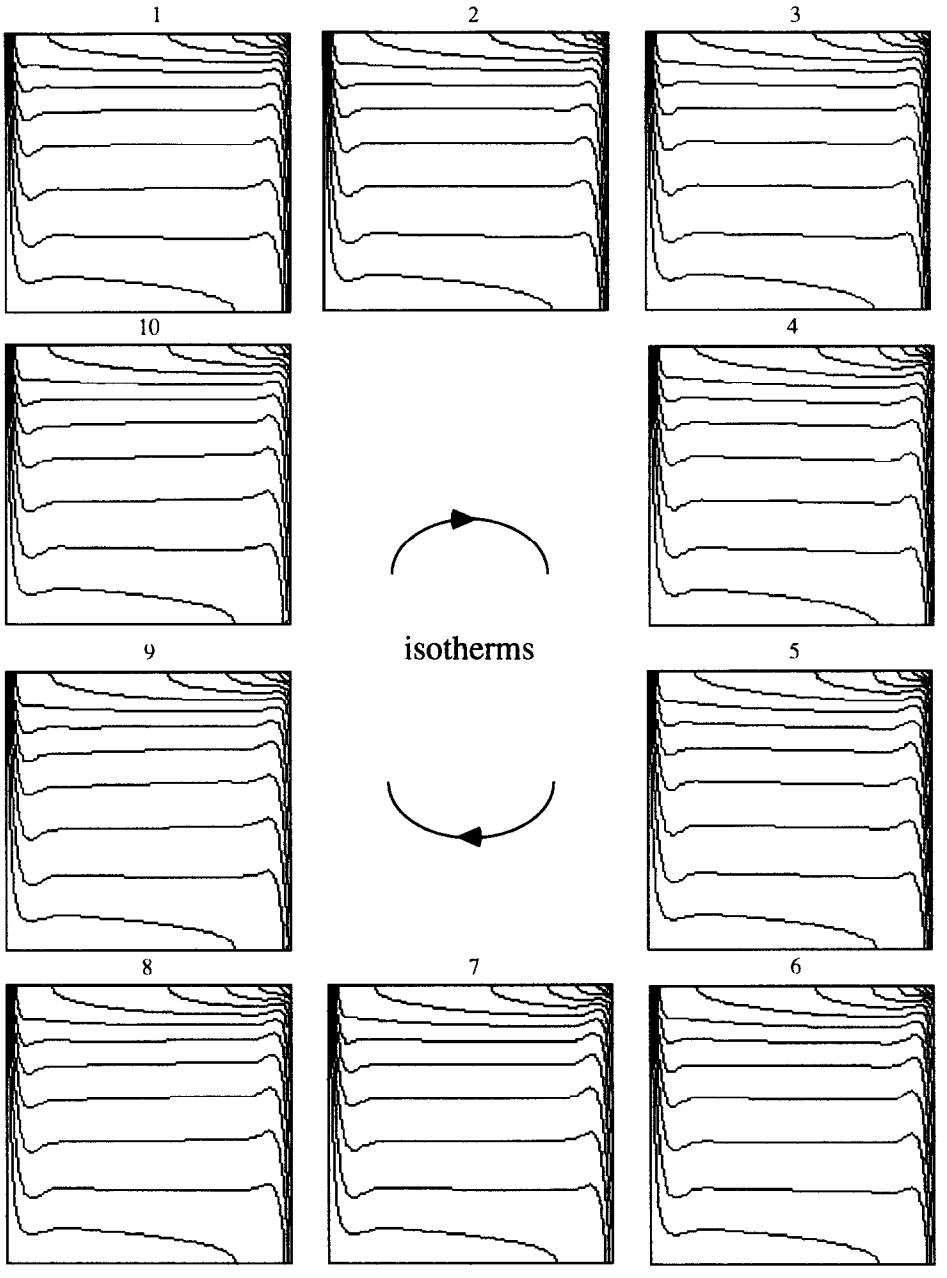

(b)

FIG. 6.—*Continued.*

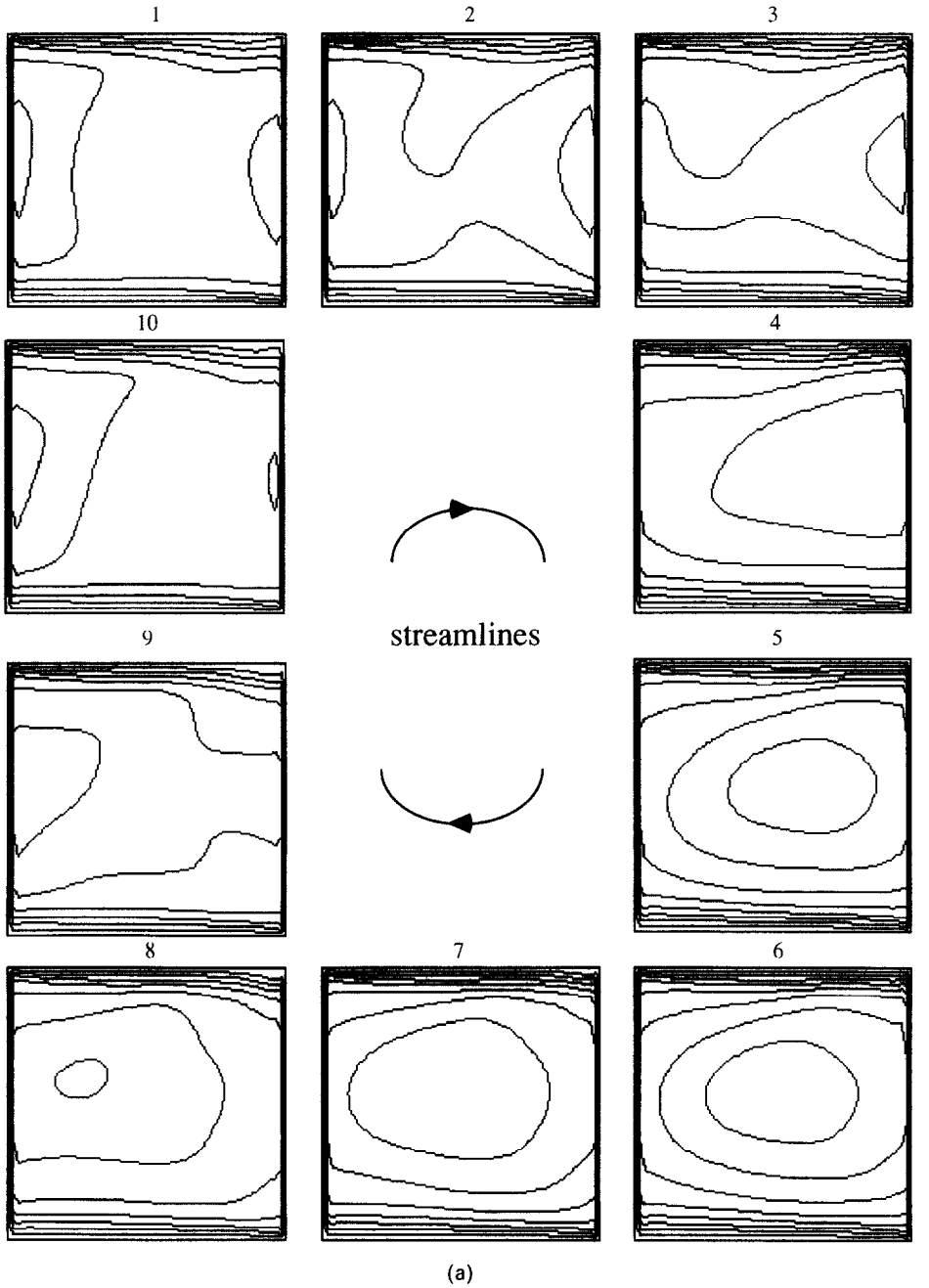

FIG. 7. Isolines from numerical simulations for $Da = 10^{-4}$, $Ra = 10^{12}$, and $F = 10^{4}$. (a) Streamlines; (b) isotherms.

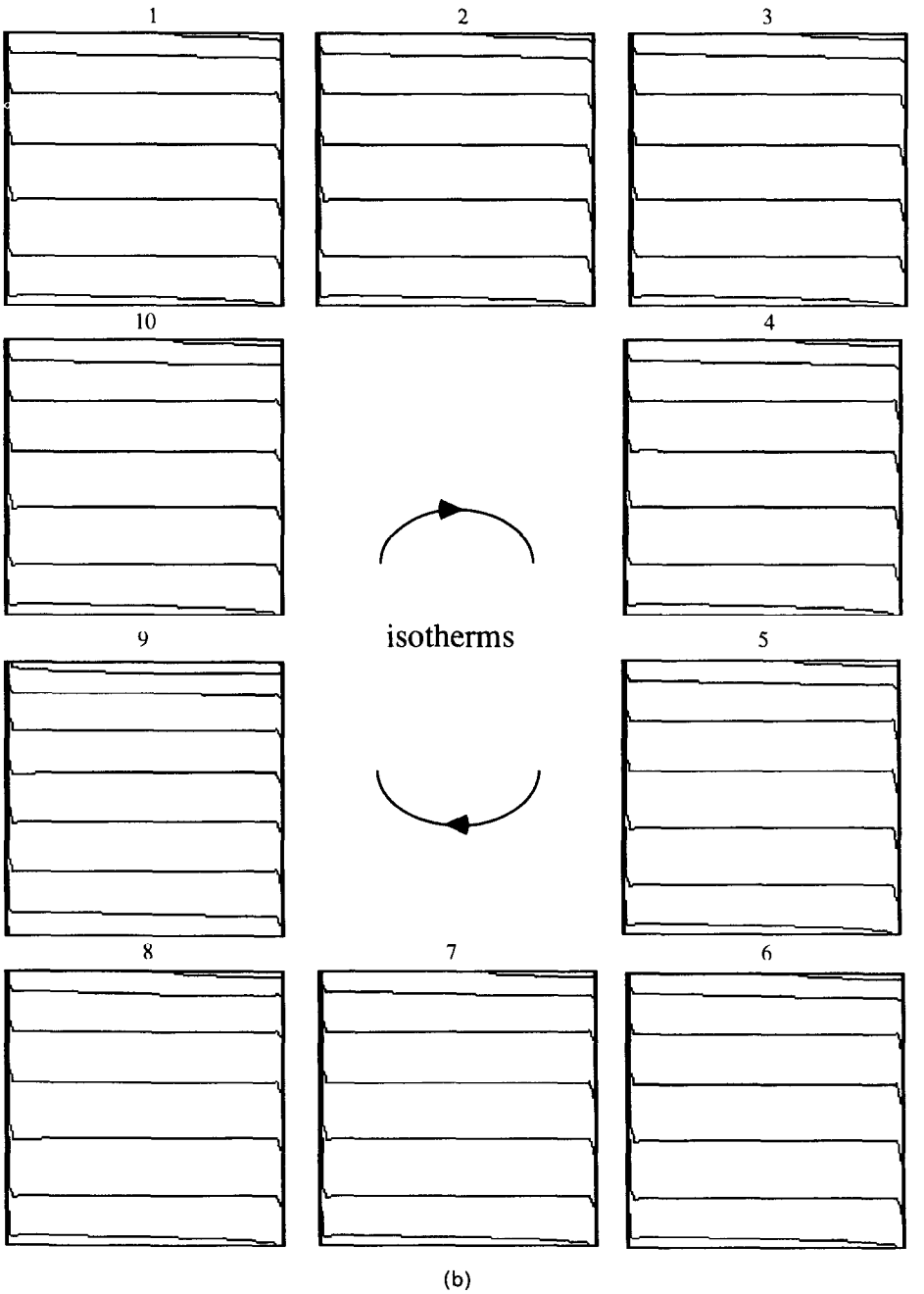

(b)

FIG. 7.—*Continued.*

an upper bound value. This might explain why the theoretical resonance frequency, equation (20), is consistently smaller than the one obtained numerically (Table 1). Interesting, and somewhat unexpectedly, Figs. 6(b) and 7(b) show very small changes in the isotherm distributions, with the core of the enclosure maintained stratified throughout the thermal process.

6. CONCLUSIONS

A general theoretical equation for predicting natural convection resonance frequency, developed on a scale basis, is proven essential to limit the exploratory frequency range for numerical simulations.

The natural convection resonance predicted physically is detected numerically by monitoring the amplitude of the enclosure mid plane heat flow. It is observed that at the resonance frequency the fluid saturated porous medium system works most efficiently as a dynamic thermal insulator, when strong natural convection activity within the system, characterized by high amplitude heat flow oscillations, coexists with a damped oscillatory heat flux at the isothermal (cold) wall.

Numerical results also support the hypothesis of resonance being more evident at high Rayleigh number (high velocities), with the minimum Ra value for resonance increasing as Da decreases. Furthermore, the present numerical simulations do not detect any resonance for small Darcy number, $Da = 10^{-6}$, even for Ra as large as 10^{13}. It is believed that at this small Darcy number, the damping introduced by the low permeability porous material inhibits the convection resonance phenomenon. Finally, the natural flow frequency (for a set of Da and Ra) can be detected numerically by simulating a case with very low input heat frequency.

Although not investigated here, the present physical reasoning indicates that increasing the heat pulsating amplitude might lead to resonance even for some of the small reference heat transfer based Rayleigh numbers used in here. This open question shall be answered in a future study.

Acknowledgements—Mr Antohe would like to express his gratitude for the Ph.D. scholarship provided by the School of Engineering and Applied Sciences of Southern Methodist University. Professor Lage's work is supported by the J. L. Embrey Professorship in Mechanical Engineering.

REFERENCES

1. J. C. Patterson and S. W. Armfield, Transient features of natural convection in a cavity, *J. Fluid Mech.* **219,** 469–497 (1990).
2. D. Poulikakos and A. Bejan, Unsteady natural convection in a porous layer, *Phys. Fluids* **26,** 1183–1191 (1983).
3. D. Poulikakos and A. Bejan, The departure from Darcy flow in natural convection in a vertical porous layer, *Phys. Fluids* **28,** 3477–3484 (1985).
4. R. J. Gross, M. R. Baer and C. E. Hickox, The application of flux-corrected transport (FCT) to high Rayleigh number natural convection in a porous medium, *Proc. Eighth Int. Heat Transfer Conf.*, San Francisco, CA, pp. 2641–2646 (1986).
5. D. A. Nield and A. Bejan, *Convection in Porous Media.* Springer, New York (1991).
6. J. L. Lage, Natural convection within a porous medium cavity: predicting tools for flow regime and heat transfer, *Int. Commun. Heat Mass Transfer* **20,** 501–513 (1993).
7. H. Q. Yang, K. T. Yang and Q. Xia, Periodic laminar convection in a tall vertical cavity, *Int. J. Heat Mass Transfer* **32,** 2199–2207 (1989).
8. M. Kazmierczak and Z. Chinoda, Buoyancy-driven flow in an enclosure with time periodic boundary conditions, *Int. J. Heat Mass Transfer* **35,** 1507–1518 (1992).
9. J. L. Lage and A. Bejan, The resonance of natural convection in an enclosure heated periodically from the side, *Int. J. Heat Mass Transfer* **36,** 2027–2038 (1993).
10. J. Mantle, M. Kazmierczak and B. Hiawy, Natural convection in a horizontal enclosure with periodic changing bottom wall temperature, *National Heat Transfer Conference*, San Diego, CA, ASME-HTD **198,** 49–56 (1992).
11. T. Yano, M. Ochi and S. Enya, Protection against fire and high temperature by using porous media and water, *ASME/JSME Thermal Engng Proc.* **4,** 213–218 (1991).
12. N. E. Wijeysundera and M. N. A. Hawlader, Effects of condensation and liquid transport on thermal performance of fibrous insulations, *Int. J. Heat Mass Transfer* **35,** 2605–2616 (1992).
13. K. Vafai and H. C. Tien, A numerical investigation of phase change effects in porous material, *Int. J. Heat Mass Transfer* **32,** 1261–1277 (1989).
14. H. Yoo and R. Viskanta, Effect of anisotropic permeability on the transport process during solidification of a binary mixture, *Int. J. Heat Mass Transfer* **35,** 2335–2346 (1992).
15. Z. Zhang and A. Bejan, The horizontal spreading of thermal and chemical deposits in a porous medium, *Int. J. Heat Mass Transfer* **30,** 2289–2303 (1987).
16. J. R. L. Skarda, Thermal modeling with solid/liquid phase change of thermal energy storage experiment, NASA-Lewis Research Center, Technical Memorandum 103770 (1991).
17. M. Chang, L. C. Chow, W. S. Chang and M. Morgan, Transient behavior of heat pipes with thermal energy storage under reversed-pulsed heat loads, *AIAA J. Thermophys. Heat Transfer* **6,** 685–692 (1992).
18. K. Vafai and C. L. Tien, Boundary and inertia effects on flow and heat transfer in porous media, *Int. J. Heat Mass Transfer* **24,** 195–203 (1981).
19. C. T. Hsu and P. Cheng, Thermal dispersion in a porous medium, *Int. J. Heat Mass Transfer* **33,** 1587–1597 (1990).
20. P. Cheng, Heat transfer in geothermal systems, *Adv. Heat Transfer* **14,** 1–105 (1978).
21. S. Ergun, Fluid flow through packed columns, *Chem. Engng Prog.* **48,** 89–94 (1952).
22. S. V. Patankar, *Numerical Heat Transfer and Fluid Flow.* Hemisphere, Washington, D.C. (1980).
23. R. A. W. M. Henkes and C. J. Hoogendorn, On the stability of natural convection flow in a square cavity heated from the side, *Appl. Scient. Res.* **47,** 195–220 (1990).
24. S. W. Armfield and J. C. Patterson, Direct simulation of wave interactions in unsteady natural convection in a cavity, *Int. J. Heat Mass Transfer* **34,** 929–940 (1991).
25. D. M. Manole and J. L. Lage, Nonuniform grid accuracy test applied to the natural convection flow within a porous medium cavity, *Numer. Heat Transfer B* **23,** 351–368 (1993).
26. J. L. Lage, On the theoretical prediction of transient heat transfer within a rectangular fluid saturated porous medium enclosure, *J. Heat Transfer* **115,** 1069–1071.